INTERNATIONAL JOURNAL OF PRECISION ENGINEERING AND MANUFACTURING Vol. 18, No. 6, pp. 813-824 JUNE 2017 / 813

REGULAR PAPER

DOI: 10.1007/s12541-017-0097-1
ISSN 2234-7593 (Print) / 2005-4602 (Online)

An Enhanced Force Bounding Approach for Stable Haptic Interaction by Including Friction

Sang-Yun Baek[1], Sangsoo Park[2], and Jeha Ryu[1,#]

1 School of Mechanical Engineering, Gwangju Institute of Science and Technology, 123, Cheomdangwagi-ro, Buk-gu, Gwangju, 61005, South Korea
2 Department of Biomedical Science and Engineering, Gwangju Institute of Science and Technology, 123, Cheomdangwagi-ro, Buk-gu, Gwangju, 61005, South Korea
Corresponding Author / E-mail: ryu@gist.ac.kr, TEL: +82-62-715-2389, FAX: +82-62-715-2384

KEYWORDS: Haptic interaction system, Passivity control, Stability, Viscous damping, Coulomb friction

There is an inherent trade-off between stability and transparency in haptic interaction systems when interacting with virtual environments. Therefore, no perfect transparency can be displayed with absolute stability. For meaningful interactions, anyhow, some level of transparency is necessary for providing realistic feelings. On the other hand, robust stability must absolutely be guaranteed against any virtual environments because unstable behaviors disrupt contact realism completely and/or may also injure human operators. In order to increase magnitude transparency of the haptic interaction system, this paper proposes a way of systematic inclusion of Coulomb friction component in the previous force bounding approach. In the inclusion, two type of force bounding approach are derived. The less conservative condition can generate significantly higher magnitude transparency in terms of the initial contact crispness as well as the steady-state contact force for very stiff virtual objects. However, there occur some contact oscillations to diminish contact realism due to the energy accumulation during free motion. In order to avoid contact oscillations, a more conservative condition is proposed for systematically removing the past accumulated energy. The proposed algorithm is also compared with the other similar algorithm. Comprehensive experimental results are presented to show the effectiveness of the proposed approaches.

Manuscript received: March 11, 2016 / Revised: January 13, 2017 / Accepted: February 24, 2017

1. Introduction

In virtual or augmented environments, haptic feedback can provide kinesthetic or tactile information about virtual objects, which in turn can offer higher levels of immersion when human operator interacts with virtual objects using haptic display devices. The haptic device is an input and output device to deliver the position date to a virtual environment and then a synthetic force or tactile information from simulated objects is displayed back to the human operator. Since haptic sensation can make subtle manipulation and exploration of virtual objects or environments, many haptic interaction techniques have been effectively used for many applications such as micro-manipulation using AFM, SEM,[1] microassembly,[2] and medical areas.[3]

In these haptic interaction systems having bi-directional energy flows, interaction stability is the most critical major requirement unlike the visual and auditory feedback systems that have only uni-directional energy flows. Unstable behaviors may cause total loss of contact realism or even may hurt human operator or may degrade contact realism. There have been many efforts to guarantee the stability; for example, the passivity-based interaction control that can be applied to various linear or nonlinear physical systems based on the input-output properties of a system.[4] Many researchers proposed stability algorithms to build stable and somewhat transparent haptic interaction systems by carefully handling energy generation.[5-9]

Some researchers found relationships between passivity and structural properties (inertia, viscous damping, Coulomb friction, sampling rate, quantization, and computational delay) of haptic display systems. Diolaiti et al. examined the stability of a haptic display by relating inertia, viscous damping, and Coulomb friction of the haptic device to controller stiffness, sampling rate, quantization, and computational delay using dimensionless parameters.[10] They were classified four stability regions as passive, locally stable, limit cycles, and unstable caused by nonlinearities of signal quantization and Coulomb friction. Their results showed that viscous damping and Coulomb friction play an important role as dissipation element in haptic interaction system. Abbott and Okamura found an explicit upper bound on the virtual wall stiffness which is a necessary and sufficient passivity condition.[11] They considered a model of haptic display having a mass with Coulomb-plus-viscous

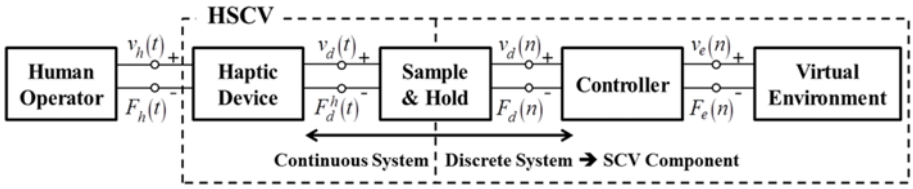

Fig. 1 Overall configuration of a haptic system: single-degree-of-freedom case from Kim et al. (Adapted from Ref. 16 with permission)

friction. Colonnese and Okamura constructed various stability and quantization-error regions for the virtual spring and damper rendering as a function of the effects of the human and device dynamics, quantization, sampling, time delay, and the low-pass filter operating on the velocity measurement.[12] They showed some necessary trade-offs that occur between parameters. However, these researches didn't present haptic controllers to stabilize the unstable haptic system caused by characteristic of virtual environment, sampling rate, quantization, and computational delay, but only showed the stable regions to design virtual spring and damper of virtual objects. This means that the virtual environment designer must know about these conditions, which is impractical because the virtual environment designers are usually different from the haptic device designers.

There is an inherent trade-off between stability and transparency in haptic interaction systems when interacting with virtual or augmented environments. Therefore, no perfect transparency can be displayed with absolute stability. For meaningful interactions, anyhow, some level of transparency is necessary for providing realistic feelings. For enhancing transparency in the haptic interaction systems, Kim et al. presented the energy-bounding algorithm (EBA) including Coulomb friction effect[10] based on the less conservative passivity condition that includes Coulomb friction explicitly. They showed that the Coulomb friction contributes to temporary increase of initial contact crispness. Lee and Lee proposed an adjusting output-limiter (AOL) algorithm for stable haptic interaction with deformable objects of unknown and/or varying impedance.[14] The AOL adjusted the maximum permissible force to guarantee passivity of the haptic system based on dissipated element by viscous damping and Coulomb friction at each sampling period. These approaches, however, may cause contact oscillations right after contacting with a very stiff virtual object because of the energy accumulation during the free-space motion.

In this paper, we propose an enhanced force bounding approach for significantly enhancing contact transparency of the haptic interaction system with any virtual environments while guaranteeing robust stability. For this purpose, the friction component in the haptic device is explicitly and systematically included in the passivity condition of sampled-data haptic systems. Since the Coulomb friction is the most dominant dissipation element at low speed cases such as when operator contacts to virtual wall, this will generate larger stiffness than only using the viscous damping at the initial contact. In the proposed approach, two types (*less* and *more*) of conditions are derived. A *less conservative condition*, the basic idea of which had been presented with only viscous damping component of the haptic device by Kim et al.,[15] can generate significantly higher transparency in terms of the initial contact crispness as well as the steady-state contact force for very stiff virtual objects. However, there exist some contact oscillations that may diminish contact realism due to the energy accumulation during free motion. In order to remove these contact oscillations, a *more conservative condition* is newly proposed for systematically removing the past accumulated energy. The proposed *less conservative condition* is turned out to be similar to that of the AOL[14] but is derived in a very simple and systematic way, which should be considered to be a theoretical contribution. Comprehensive experimental results are presented to show the effectiveness of the proposed approaches. In order to check the increase of transparency by including Coulomb friction, the user-study is performed.

The remaining part of the paper is organized as follows: section 2 summarizes the passivity condition of a haptic system that is modeled as a sampled-data system including Coulomb friction of haptic device. In section 3, *less* and *more conservative passivity conditions* for haptic interaction systems are derived. Experimental results are presented in section 4 to verify that the proposed approaches make the haptic interaction passive. We also perform the experimental comparison with AOL. Section 5 then presents psychophysical study. The paper concludes and provides future works in Section 6.

2. Passivity Condition for a Sampled-Data System Including Coulomb Friction

In this section, the passivity condition of a sampled-data haptic interaction system including Coulomb friction is briefly summarized to understand proposed approach. Fig. 1 shows the overall configuration of a haptic system with a single-DOF device from Kim et al..[15] General haptic system is composed of a haptic device, a controller, and a virtual environment. The haptic device, which is input and output electro-mechanical system to deliver the calculated position and force information, can allow the human operator intuitively and naturally to touch, to explore, and to manipulate a virtual object in the virtual environment. The virtual environment contains a haptic rendering algorithm which detects a collision between the avatar (representing, for example, a fingertip) and virtual objects and then compute collision responses (contact forces/torques). The controller denotes any algorithm to connect the haptic device to virtual objects.

In the haptic interaction system, a sample-and-hold operator, which is usually a zero-order holder (ZOH), is used to connect the discrete system to the continuous system. The loss of information in the sampling and the half sample delay in the ZOH can make the haptic system active, which may result in unstable haptic interaction. A goal of passivity-based control is to make the haptic system passive, which does not generate energy to destabilize the system. In order to guarantee a passive haptic interaction system with human operators who are assumed to be passive while manipulating the haptic device, the energy

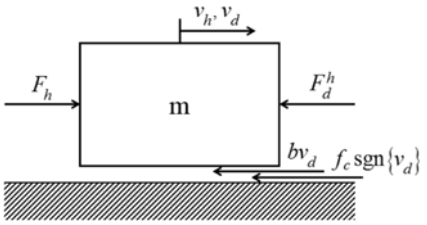

Fig. 2 Schematic of the haptic interface model

flow-in ($E(n)$) to the one-port system in Fig. 1 should not be negative such that:

$$E(n) = \int_0^t F_h(\tau) v_h(\tau) d\tau \geq 0 \quad \text{for } t > 0 \text{ and all admissible } F_h(t), \tag{1}$$

where $F_h(t)$ and $v_h(t)$ represent applied force and velocity by a human operator, respectively. Note here that all the initial conditions are assumed to be zero for simple mathematical derivations without loss of generalities.

For a single-DOF device with mass (m), viscous damping (b), Coulomb friction (f_c) elements, dynamic relations are:

$$F_h(t) = m\dot{v}_h(t) + bv_h(t) + f_c \operatorname{sgn}\{v_d(t)\} + F_d^h(t), \tag{2}$$

$$v_h(t) = v_d(t). \tag{3}$$

where $F_d^h(t)$ and $v_d(t)$ represent hold actuator force by the digital-to-analog converter and velocity of the haptic device as shown in Fig. 2.

The energy flow-in to the system can be rewritten for the single-DOF haptic device during $0 \leq t < nT$ as:

$$E(n) = \int_0^{nT} m\dot{v}_d(t) v_d(t) dt + \int_0^{nT} bv_d^2(t) dt + \int_0^{nT} f_c \operatorname{sgn}\{v_h(t)\} v_d(t) dt + \int_0^{nT} F_d^h(t) v_d(t) dt \geq 0.$$

The third term in Eq. (4) indicate the energy dissipation by the Coulomb friction. It can be rewritten using triangle inequality[10] as:

$$\begin{aligned} \int_0^{nT} f_c \operatorname{sgn}\{v_d(t)\} v_d(t) dt &= \int_0^{nT} f_c |v_d(t)| dt \\ &= \sum_{k=0}^{n-1} \left\{ f_c \int_{kT}^{(k+1)T} |v_d(t)| dt \right\} \geq \sum_{k=0}^{n-1} \left\{ f_c \left| \int_{kT}^{(k+1)T} v_d(t) dt \right| \right\} \\ &= \sum_{k=0}^{n-1} f_c |\Delta x_d(k+1)|. \end{aligned} \tag{5}$$

where $\Delta x_d(k+1) = [x_d(k+1) - x_d(k)]$. Note that $\Delta x_d(k+1)$ denotes the position difference of the device between samples. The other terms are derived in the previous paper.[15]

The energy flow-in to the during $0 \leq t < nT$ in Eq. (1) can then be rewritten as:

$$E(n) \geq E_1(n) = \sum_{k=0}^{n-1} B\Delta x_d^2(k+1) + \sum_{k=0}^{n-1} f_c |\Delta x_d(k+1)| + \sum_{k=0}^{n-1} F_d(k) \Delta x_d(k+1) \geq 0. \tag{6}$$

where $B = b/T$ implies energy dissipation capability by viscous damping of the haptic device between samples. Note that the condition in Eq. (6) ($E_1(n) \geq 0$) is a sufficient condition for the original passivity condition in Eq. (4) ($E(n) \geq 0$) due to the inequality condition at the energy dissipation elements in viscous damping and Coulomb friction, and due to neglect of the kinetic energy.

There are several other energy generation factors in the SCV subsystem: computation delay, explicit integration in simulating the virtual environment, non-zero phase lag in position or velocity filters, communication delays when a haptic device is connected to the virtual environment by a network, and the gravity or friction compensation algorithms. These factors can make the SCV subsystem active; in other words, the forth term of Eq. (6) can be negative. In order to guarantee the passivity condition which can make the energy of haptic system non-negative in Eq. (6), the actuator control command force $F_d(k)$ should be carefully planned.

3. Force Bounding Approach

This section presents how the actuator control command force $F_d(k)$ can be designed such that the passivity condition in Eq. (9) is satisfied for any virtual environments. For this, *less* and *more conservative conditions* will be discussed to make the haptic system passive. Subsection 3.1 derives a *less conservative condition* from Eq. (6). A *more conservative condition* is then derived in subsection 3.2 in order to remove severe contact oscillations that may result from the *less conservative condition* due to accumulated energy from the motion before virtual object contact.

3.1. Less conservative condition for passivity

The actuator control command force $F_d(k)$ decided at $t = nT$ should guarantee the passivity condition until the next time step (*i.e.*, $t < (n + 1)T$). Thus, $F_d(k)$ should make $E_1(n + 1)$ in Eq. (6) non-negative for passivity as:

$$E_1(n+1) = B\Delta x_d^2(n+1) + f_c |\Delta x_d(n+1)| + F_d(n) \Delta x_d(n+1) + E_1(n). \tag{7}$$

Proposition 1: Conservative Sufficient Condition of $F_d(n)$.

For all possible $\Delta x_d(n + 1)$, the passivity condition in Eq. (7) is satisfied if and only if

$$\sum_{k=0}^{n-1} B\Delta x_d^2(k+1) + \sum_{k=0}^{n-1} f_c |\Delta x_d(k+1)| + \sum_{k=0}^{n-1} F_d(k) \Delta x_d(k+1) \geq \frac{F_d^2(n)}{4B} - f_c |\Delta x_d(n+1)|. \tag{8}$$

Proof: For positive dissipation $B > 0$, the passivity condition in Eq. (7) can be rewritten as:

$$\frac{1}{4B} \{2B\Delta x_d(n+1) + F_d(n)\}^2 - \frac{F_d^2(n)}{4B} + f_c |\Delta x_d(n+1)| + E_1(n) \geq 0. \tag{9}$$

The condition Eq. (9) is satisfied if and only if the minimum value of the left side of Eq. (10) for all $\Delta x_d(n + 1)$ is non-negative as:

$$E_1(n) - \frac{F_d^2(n)}{4B} + f_c |\Delta x_d(n+1)| \geq 0. \tag{10}$$

From the definition of $E_1(n)$ in Eq. (6), the condition Eq. (10) can

be rewritten as Eq. (8).

To make a haptic system passive, the actuator control command force should satisfy the condition in Eq. (8) for all n. Note that a similar result had been derived in AOL algorithm[14] through more complex arguments.

In order to satisfy the *less conservative condition* of $F_d(n)$ for the passivity in Eq. (8), the following force bounding rule is proposed in this paper:

$$\begin{aligned} E_1(n) = E_1(n-1) + B\Delta x_d^2(n) \\ + f_c\left|\Delta x_d(n)\right| + F_d(n-1)\Delta x_d(n), \end{aligned} \tag{11}$$

$$\begin{aligned} F_{\max}(n) &= \sqrt{4B\left\{E_1(n) + f_c\left|\Delta x_d(n+1)\right|\right\}}, \\ F_{\min}(n) &= -\sqrt{4B\left\{E_1(n) + f_c\left|\Delta x_d(n+1)\right|\right\}}, \end{aligned} \tag{12}$$

$$\begin{aligned} &if\left(F_e(n) > F_{\max}(n)\right) && F_d(n) = F_{\max}(n) \\ &else\ if\left(F_e(n) < F_{\min}(n)\right) && F_d(n) = F_{\min}(n) \\ &else && F_d(n) = F_e(n) \end{aligned} \tag{13}$$

where $F_e(n)$ is the force computed in the virtual environment. If $F_e(n)$ is within the bands, then the proposed algorithm provides full transparency. Note that the negative $F_{min}(n)$ can be the case for pulling the virtual spring in the bilateral connection to the virtual spring.

This controller, although it guarantees the passivity condition of the haptic system, requires the future position difference information $\Delta x_d(n + 1)$ in Eq. (12). In order to avoid or circumvent this causality problem, we approximate the controlled force ranges in Eq. (12) as those in Eq. (14), which is, in fact, similar to the method in the "Passive-Set-Position-Modulation (PSPM)[9]

$$\begin{aligned} F_{\max}(n) &= \sqrt{4B\left\{E_1(n) + f_c\left|\Delta x_d(n)\right|\right\}}, \\ F_{\min}(n) &= -\sqrt{4B\left\{E_1(n) + f_c\left|\Delta x_d(n)\right|\right\}}. \end{aligned} \tag{14}$$

Note that this substitution of $\Delta x_d(n + 1)$ by $\Delta x_d(n)$ may not cause any stability problem even though the position is affected by the controlled force and vice versa. This is because the computed values in Eq. (14) are almost the same as those in Eq. (12) due to a very fast sampling time (usually 1 *kHz*) as well as because the proposed passivity condition is very conservative condition for stability. One drawback of this approximation, however, reduces transparency because the dissipation capability by the Coulomb friction is computed by the current information instead of future information. Degradation of transparency, however, may not be serious by this approximation because $\Delta x_d(n + 1)$ is very similar to $\Delta x_d(n)$ in most contacts for very fast sampling, which will be experimentally validated in subsection 4.3.

3.2 More conservative condition for passivity

The *less conservative condition* in Eq. (8) provides less conservative force, guaranteeing the passivity. Note that the first term ($\Sigma B\Delta x_d^2(k + 1)$) and the second term ($\Sigma f_c|\Delta x_d(k + 1)|$) of the energy $E_1(n)$ in Eq. (9) is the sum of the dissipation capability during all the interaction time. This accumulated energy induces a *memory effect* that may deteriorate contact realism. If, for example, a user moves in free space for a long time before contacting a virtual object, the accumulated energy may have a larger value before contact. Upon contact, the accumulated dissipation capability allows active behavior until it is counterbalanced by the generated energy. This *memory effect* may induce severe oscillations (that will be shown in the experimental results in the later section) and thus may not be acceptable for some applications requiring realistic contact transparency such as in medical simulators. Thus, a careful reset process of the accumulated dissipation capability may be required to avoid severe oscillatory behaviors during specific time period.

A simple way to derive the *memoryless* type of the force condition for passivity is to neglect the previous remaining dissipation capability. In order to derive this control, we change the passivity condition in Eq. (6) to the following condition as:

$$\begin{aligned} E_2(n) \equiv \sum_{k=0}^{n-1}\beta(k)\Delta x_d^2(k+1) + \sum_{k=0}^{n-1} f_c\left|\Delta x_d(k+1)\right| \\ + \sum_{k=0}^{n-1} F_d(k)\Delta x_d(k+1) \ge 0, \end{aligned} \tag{15}$$

where $0 < \beta(k) \le B$ for all $k \in [0, n–1]$. Note that the condition Eq. (15) is sufficient for the condition Eq. (6) ($E_1(n) \ge E_2(n)$), therefore, it is called *more conservative condition*. Note also that the conditions Eqs. (6) and (15) become exactly the same as each other when we choose $\beta(k) = B$ for all $k \in [1, n - 1]$.

In order that the actuator control command force $F_d(n)$ decided at $t = nT$ guarantees the passivity condition until the next time step, $F_d(n)$ should make $E_2(n + 1)$ non-negative for passivity as:

$$\begin{aligned} E_2(n+1) = \beta(n)\Delta x_d^2(n+1) + f_c\left|\Delta x_d(n+1)\right| \\ + F_d(n)\Delta x_d(n+1) + E_2(n) \ge 0. \end{aligned} \tag{16}$$

Proposition 2: More Conservative Condition of $F_d(n)$.

For all possible values of unknown $\Delta x_d(n+1)$, the passivity condition in Eq. (16) is satisfied if and only if

$$\begin{aligned} \frac{1}{\beta(i-1)}\left\{2\beta(i-1)\Delta x_d(i) + F_d(i-1)\right\}^2 \\ \ge \frac{F_d^2(i)}{\beta(i)} - 4f_c\left|\Delta x_d(i+1)\right|. \end{aligned} \tag{17}$$

for all the interaction time n.

Proof: It can easily be shown that for all possible $\Delta x_d(n+1)$, the condition in Eq. (16) is satisfied if and only if

$$\begin{aligned} \sum_{k=0}^{n-1}\beta(k)\Delta x_d^2(k+1) + \sum_{k=0}^{n-1} f_c\left|\Delta x_d(k+1)\right| \\ + \sum_{k=0}^{n-1} F_d(k)\Delta x_d(k+1) \ge \frac{F_d^2(n)}{4\beta(n)} - f_c\left|\Delta x_d(n+1)\right|. \end{aligned} \tag{18}$$

The right side of Eq. (18) can be rewritten (assume $F_d(0) = 0$, $\Delta x_d(1) = 0$) as:

$$\begin{aligned} \frac{F_d^2(n)}{4\beta(n)} - f_c\left|\Delta x_d(n+1)\right| \\ = \sum_{k=0}^{n-1}\frac{F_d^2(k+1)}{4\beta(k+1)} - \sum_{k=0}^{n-1}\frac{F_d^2(k)}{4\beta(k)} \\ - \sum_{k=0}^{n-1} f_c\left|\Delta x_d(k+2)\right| + \sum_{k=0}^{n-1} f_c\left|\Delta x_d(k+1)\right|. \end{aligned} \tag{19}$$

Then, the condition in Eq. (18) can be rewritten as:

$$\sum_{k=0}^{n-1}\left[\frac{\left\{2\beta(k)\Delta x_d(k+1)+F_d(k)\right\}^2}{4\beta(k)} - \frac{F_d^2(k+1)}{4\beta(k+1)}+f_c\left|\Delta x_d(k+2)\right|\right]\geq 0. \tag{20}$$

If the actuator force $F_d(i)$ satisfies the following condition for all $i \in [1, n]$ as:

$$\frac{1}{4\beta(i-1)}\left\{2\beta(i-1)\Delta x_d(i)+F_d(i-1)\right\}^2 \geq \frac{F_d^2(i)}{4\beta(i)}-f_c\left|\Delta x_d(i+1)\right|. \tag{21}$$

Then, the left side of Eq. (20) has a non-negative value for each k, and thus the condition in Eq. (18) is satisfied.

Note that there always exists a possible region of $F_d(n)$ for satisfying the condition Eq. (17) since the left side of Eq. (17) always has non-negative value. Note also that, unlike Eq. (8), the condition of Eq. (17) does not contain the sum of previous states; thus, it releases the *memory effect* during specific time periods.

There exist two factors that the sufficient condition of $F_d(n)$ in Eq. (17) provides a more conservative force region guaranteeing the passivity condition in Eq. (6): (i) the dissipation $\beta(k) \in (0, B]$ is used to describe passivity condition in Eq. (16) instead of using B in Eq. (7). (ii) The condition Eq. (17) makes each term of Eq. (20) non-negative, therefore the total sum of Eq. (20) is non-negative.

However, this conservatism is necessary to ignore the previous remaining dissipations capability. For example, if a user interacts with a soft virtual object in which the dissipation capability is sufficient for the actuator force $F_d(i)$ to be displayed exactly with the satisfaction of Eq. (21), the remaining dissipation can easily be rejected by using required dissipation $\beta(i) \in (0, B]$ as

$$\gamma(i)=2\beta(i-1)\Delta x_d(i)+F_d(i-1), \tag{22}$$

$$\rho(i)=4\beta(i-1)f_c\left|\Delta x_d(i+1)\right|, \tag{23}$$

$$\beta(i)=\frac{F_d^2(i)\beta(i-1)}{\gamma^2(i)+\rho(i)} \quad for \quad F_d(i)\neq 0. \tag{24}$$

Then, the total sum of Eq. (20) in the previous states becomes zero (*i.e.*, previous remaining dissipation is rejected), and thus the solution to make the current term of Eq. (20) non-negative is identical to the solution to make the total sum non-negative.

If the user now moves and interacts with a very stiff virtual object in which the dissipation capability is not enough so that the actuator force $F_d(i)$ cannot be displayed fully (*i.e.*, $F_d(i) < F_e(i)$) (in which case the dissipation capability $\beta(i)$ will be selected to be B), the actuator force $F_d(i)$ needs to be saturated for the passivity such that

$$F_d^2(i)=\frac{\beta(i)}{\beta(i-1)}\left\{2\beta(i-1)\Delta x_d(i)+F_d(i-1)\right\}^2 + 4\beta(i-1)f_c\left|\Delta x_d(i+1)\right|. \tag{25}$$

Then, the total sum of Eq. (20) in the previous states becomes zero (*i.e.*, there is no remaining dissipation), and thus the solution to make the current term of Eq. (20) non-negative is identical to the solution to make the total sum non-negative.

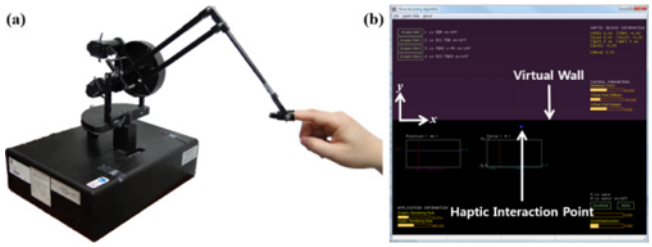

Fig. 3 (a) PHANToM Premium 1.5, (b)Virtual Wall

In order to satisfy the *more conservative condition* of $F_d(i)$ in Eq. (17), the following force bounding rule is proposed:

$$\gamma(n)=2\beta(n-1)\Delta x_d(n)+F_d(n-1), \tag{26}$$

$$\rho(n)=4\beta(n-1)f_c\left|\Delta x_d(n+1)\right|, \tag{27}$$

$$\beta(n)=\frac{F_e^2(n)}{\gamma^2(n)+\rho(n)}\beta(n-1) \quad for \quad F_e(n)\neq 0, \tag{28}$$

$$if\left(\beta(n)>B\right) \quad \beta(n)=B, \tag{29}$$

$$F_{\max}(n)=\sqrt{\frac{\beta(n)}{\beta(n-1)}\left\{\gamma^2(n)+\rho(n)\right\}}, \quad F_{\min}(n)=-\sqrt{\frac{\beta(n)}{\beta(n-1)}\left\{\gamma^2(n)+\rho(n)\right\}}, \tag{30}$$

In the above bounding rule, the required dissipation capability $\beta(n)$ in Eq. (28) is computed first to display the desired force $F_e(n)$ transparently. If the required dissipation $\beta(n)$ in Eq. (28) exceeds the available dissipation capability B, then $\beta(n)$ is limited to B as in Eq. (29). The initial value of $\beta(n)$ is set to B.

The controller in Eq. (30) has also causality problem, which need the future position information to compute stable force range, so we approximate the condition Eq. (27) such that

$$\rho(n)=4\beta(n-1)f_c\left|\Delta x_d(n)\right|, \tag{31}$$

Note that the modified $\rho(n)$ in Eq. (31) can also guarantee passivity, again because this condition is also very conservative condition for stable haptic system. This is also experimentally validated in subsection 4.3.

4. Experiments

This section presents simulation and experimental results to show that the proposed algorithm can enhance significantly the haptic interaction transparency while guaranteeing robust stability. We also show an experimental comparison between the proposed approach and the AOL. Finally, the experimental results in subsection 4.3 show that the approximated controllers in Eqs. (14) and (30) are in fact do not cause any substantial stability and transparent degradation.

4.1 Experimental setup

This section presents experimental procedures and results with a

commercial 3-DOF haptic device, the PHANToM Premium 1.5 as shown in Fig. 3(a). The maximum force exertion is 8.5 *N* and the encoder resolution is 0.03 *mm* at the nominal position.[17] The proposed approach is implemented using the Microsoft Visual Studio 2010 operating in Windows XP. A sampling rate of about 1 *kHz* is used by the OpenHaptic Thread. The minimum Coulomb friction (f_c) and viscous damping (b) at y-axis are identified as 0.12 *N* and 0.27 *Ns/m*.[14]

The following virtual wall model is used:

$$F_e(n)=\begin{cases} k\{x_d(n)-x_{wall}\} & x_d(n)\geq x_{wall} \text{ for normal wall} \\ (k_1+k_2 t)\{x_d(n)-x_{wall}\} & x_d(n)\geq x_{wall} \text{ for time varying} \\ 0 & x_d(n)<x_{wall} \end{cases} \quad (32)$$

where x_{wall} is the position of the virtual wall that is located at x_{wall} = 10 *mm*.

For objective comparison among various approaches (the proposed enhanced FBA, the previous FBA, AOL, *etc.*), two transparency measures are compared: (i) Steady-state contact stiffness that can be defined as the displayed stiffness that is the actual stiffness felt by the operator:

$$S_D=\frac{Controlled\ force\ (N)}{Penetration\ depth\ (mm)}. \quad (33)$$

(ii) The crispness in the transient state of contact with virtual wall can be defined as using the rate-hardness defined by Lawrence as[18]

$$H_R=\frac{Initial\ force\ rate\ of\ change\ (N/s)}{Initial\ penetration\ velocity\ (m/s)}. \quad (34)$$

In the experiments, two different approaching velocities (high and low) are used because the position difference term $\Delta x_d(n)$ (representing velocity) may be affected by the resolution (0.03 *mm*/0.001 *s* = 30 *mm/sec*) at the end effector of the haptic device. Furthermore, the grip is controlled to be a soft grip for all experiments in order to avoid the human damping effect on the stability and transparency.

4.2 Experimental results

Figs. 4, 5 and 6 show experimental results for the time varying system (k_1 = 0.3 *N/mm*, k_2 = 0.06 *N/mm·s*) with the *less conservative conditions* (Eqs. (11) to (14)), with the *more conservative conditions* (Eqs. (26) to (31)), and with the AOL. All controllers can display transparently the full stiffness in the time varying system because the wall stiffness lies in the range of dissipation capability of the haptic device by the viscous damping and Coulomb friction.

Fig. 7 shows experimental results for the virtual wall with large stiffness (k = 10 *N/mm*) at y-axis when no control law is applied ($F_d(n)$ = $F_e(n)$). This figure shows clear instability in the position and force histories as well as negative energy behavior.

Figs. 8 and 9 show experimental results for the same virtual wall with stiffness k = 10 *N/mm* when the previous *less conservative* FBA[12] having only viscous damping term is applied at high and low velocities. Here, the following force bounding rule is used:

$$E_1'(n)=E_1'(n-1)+B\Delta x_d^2(n)+F_d(n-1)\Delta x_d(n), \quad (35)$$

$$F_{max}(n)=\sqrt{4BE'_1(n)}$$
$$F_{min}(n)=-\sqrt{4BE'_1(n)} \quad (36)$$

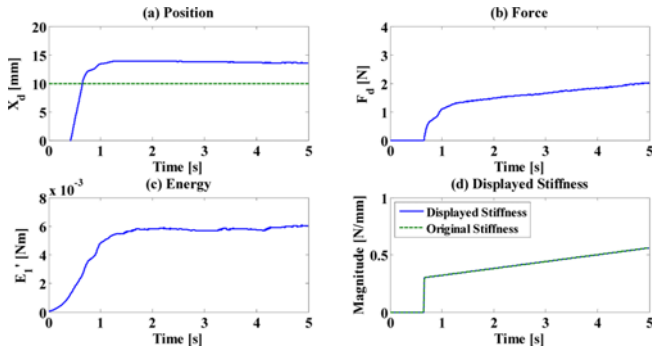

Fig. 4 Experimental results for time varying system (k_1 = 0.3 N/mm, k_2 = 0.06 N/mm·s) with a *less conservative condition* using viscous damping and Coulomb friction

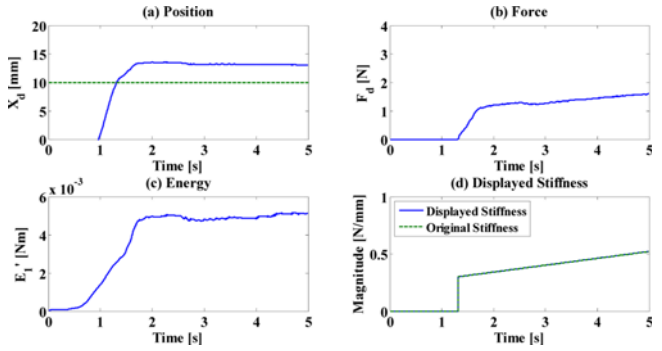

Fig. 5 Experimental results for time varying system (k_1 = 0.3 N/mm, k_2 = 0.06 N/mm·s) with a *more conservative condition* using viscous damping and Coulomb friction

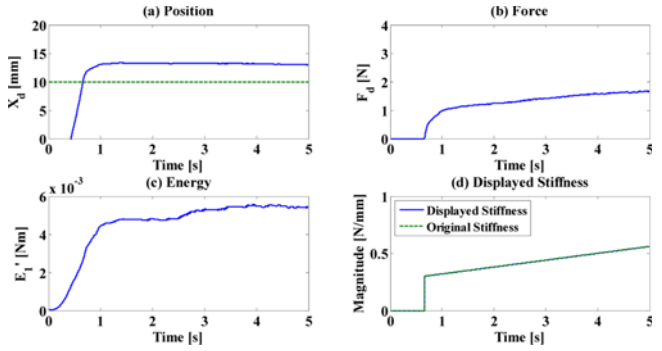

Fig. 6 Experimental results for time varying system (k_1 = 0.3 N/mm, k_2 = 0.06 N/mm·s) with the adjusting output-limiter[14]

Unlike the experiment results without any controller at large stiffness virtual wall in Fig. 7, it is possible to stably touch the virtual wall as shown in Figs. 8 and 9 because the bounding laws in Eq. (20) had been active in this case.

The rate-hardness, which is the crispness measure of contact with a stiff virtual wall in Eq. (34), is 3.06 *N/mm* in Fig. 8(e) and 7.87 *N/mm* in Fig. 9(e). The displayed stiffness in Eq. (33) is measured at the steady-state (averaged value during 2~5 seconds) 0.71 *N/mm* in Fig. 8(e) and 0.69 *N/mm* in Fig. 9(e). Notice that the rate-hardness value of the low speed is larger than that of the high speed because the accumulated

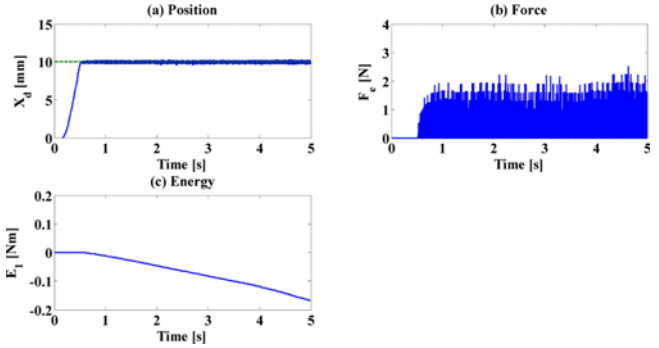

Fig. 7 Experimental results for large stiffness (k = 10N/mm) without any controller

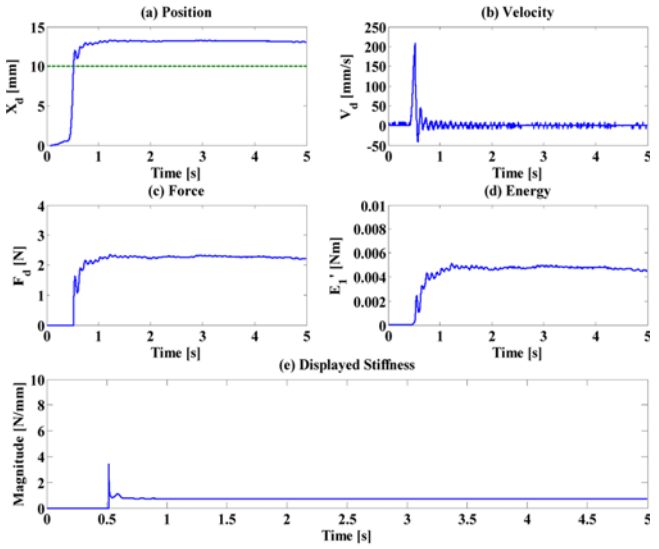

Fig. 8 Experimental results for large stiffness (k = 10 N/mm) with a *less conservative condition* including viscous damping and Coulomb friction at high velocity

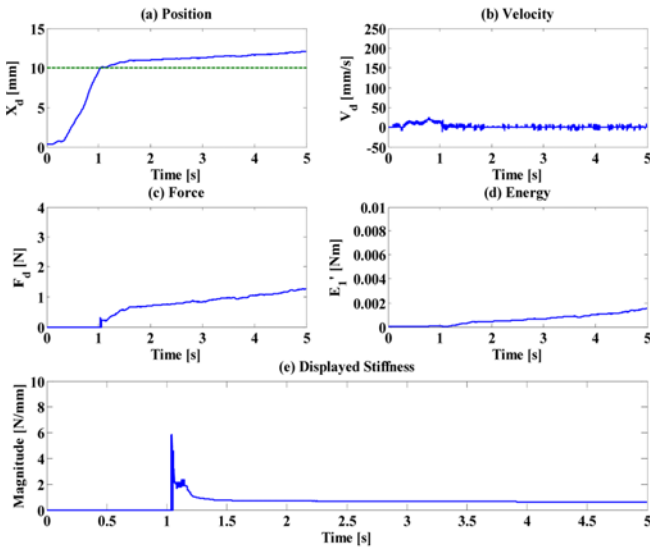

Fig. 9 Experimental results for large stiffness (k = 10 N/mm) with a *less conservative condition* including viscous damping and Coulomb friction at low velocity

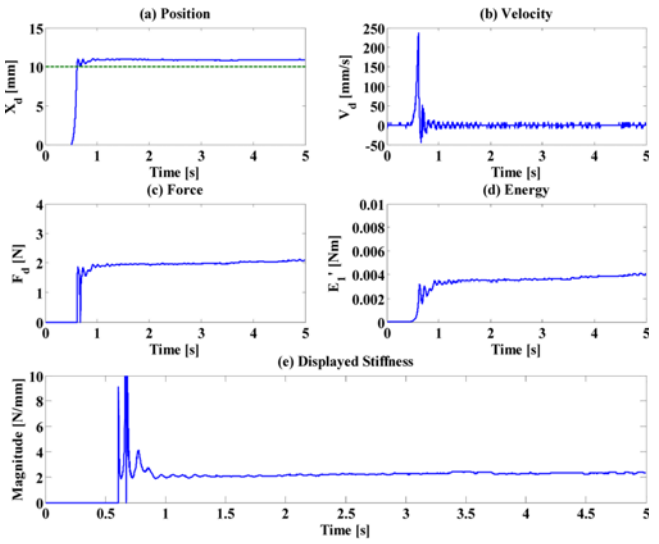

Fig. 10 Experimental results for large stiffness (k = 10 N/mm) with a *less conservative condition* including viscous damping and Coulomb friction at high velocity

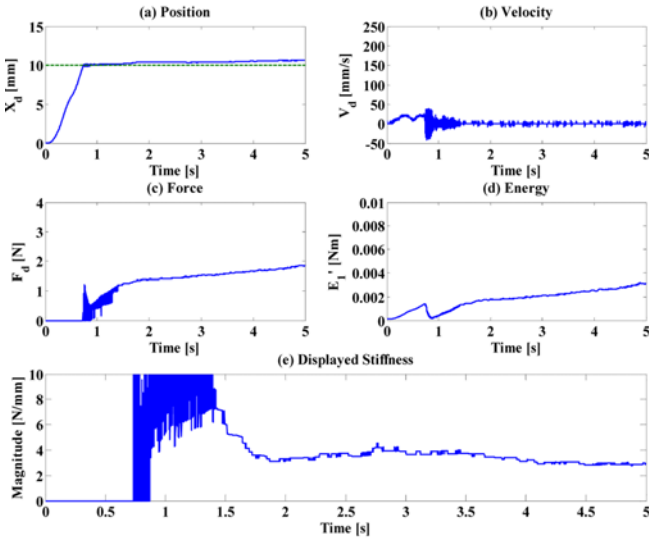

Fig. 11 Experimental results for large stiffness (k = 10 N/mm) with a *less conservative condition* including viscous damping and Coulomb friction at low velocity

energy before contact is larger (due to more time to reach to the wall) in the low speed. Some oscillations can be clearly felt after initial contact as shown in Fig. 9(c) because the energy is accumulated by the viscous damping during free-space movement at low velocity case ($1.278\ sec \le t \le 1.339\ sec$). This severe oscillation can deteriorate the initial contact feeling.

Figs. 10 and 11 show experimental results for the virtual wall with stiffness k = 10 *N/mm* when the proposed *less conservative condition* including both viscous damping and Coulomb friction at high and low velocities. These Figs. show clearly that both transparency in the transient and the steady-state phases is increased significantly by the inclusion of Coulomb friction term as shown in Figs. 10(e) and 11(e) when compared with the previous FBA with only viscous damping as

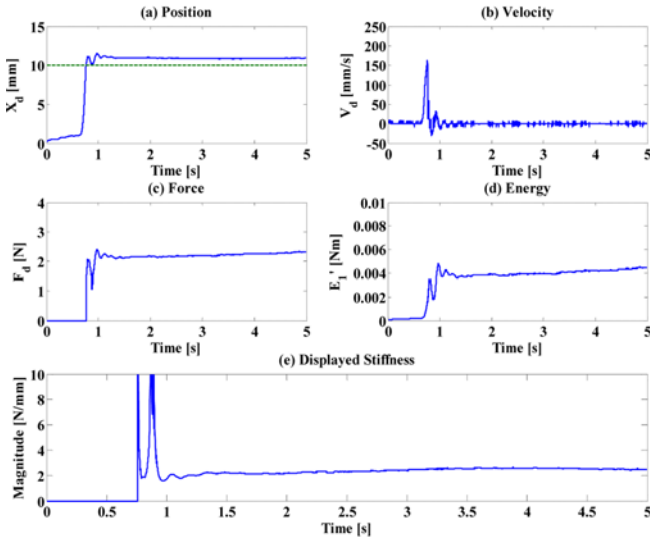

Fig. 12 Experimental results for large stiffness (k = 10 N/mm) with an adjusting output-limiter at high velocity

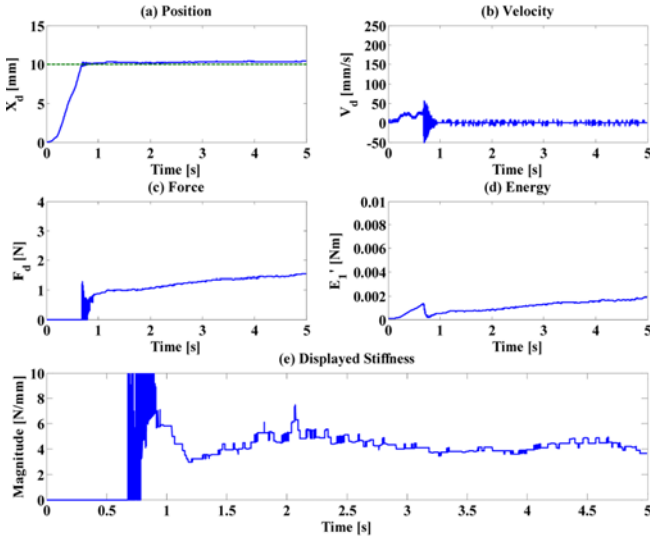

Fig. 13 Experimental results for large stiffness (k = 10 N/mm) with an adjusting output-limiter at low velocity

shown in Figs. 8(e) and 9(e). (For the displayed stiffness: 2.28 *N/mm* and 4.09 *N/mm* in Figs. 10(e) and 11(e), respectively vs. 0.71*N/mm* in Fig. 8(e) and 0.69*N/mm* in Fig. 9(e), respectively. For the rate-hardness: 6.05 *N/mm* and 8.02 *N/mm* in Figs. 10(e) and 11(e), respectively vs 3.06 *N/mm* in Fig. 8(e) and 7.87 *N/mm* in Fig. 9(e), respectively). It also shows severe oscillations due to the energy accumulated by the Coulomb friction as well as viscous damping before virtual wall contact.

Compare the proposed *less conservative* approach with the AOL approach, Figs. 12 and 13 show the experimental results for the virtual environment with a large stiffness k = 10 *N/mm* at high and low velocities. The rate-hardness is 6.02 *N/mm* and 8.25 *N/mm*. The displayed stiffness is 2.47 *N/mm* and 4.44 *N/mm*. These values are very similar with those (2.28 *N/mm* and 4.09 *N/mm* in Figs. 10(e) and 11(e)) of the proposed *less conservative condition* including viscous damping and Coulomb friction. This approach also shows severe oscillations after initial contact due to the energy accumulated during free motion.

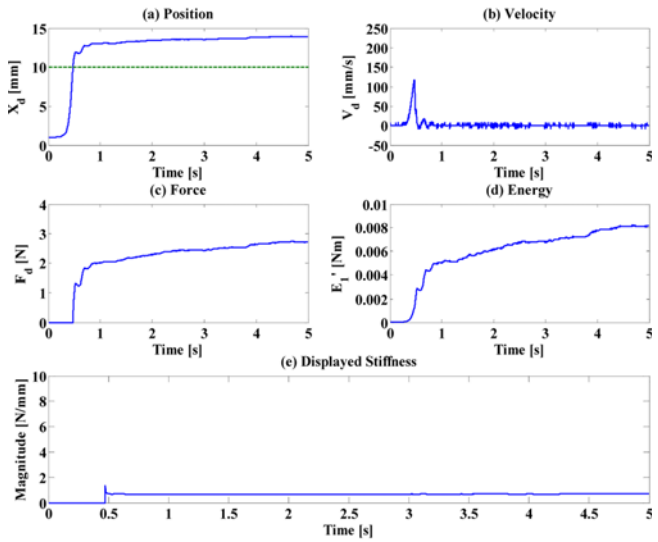

Fig. 14 Experimental results for large stiffness (k = 10 N/mm) with a *more conservative condition* including viscous damping and Coulomb friction at high velocity

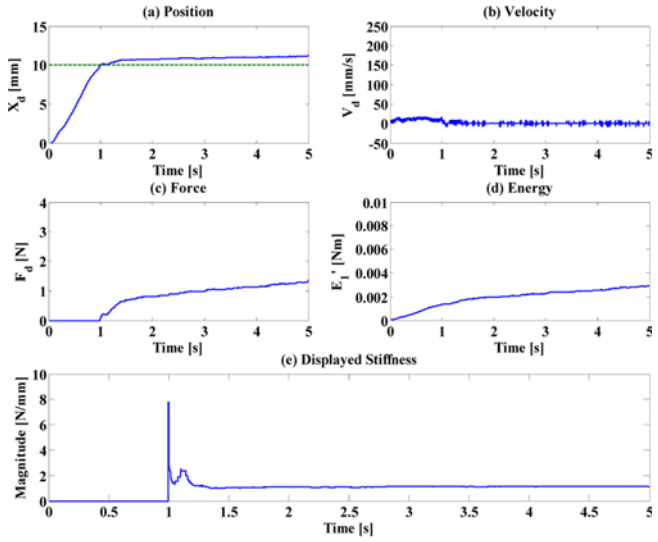

Fig. 15 Experimental results for large stiffness (k = 10 N/mm) with a *more conservative condition* including viscous damping and Coulomb friction at low velocity

In order to remove the severe oscillations at the initial contact, the proposed *more conservative condition* is applied with the same experimental conditions. Figs. 14 and 15 show no severe oscillations as expected because the *more conservative condition* does not show the *memory effect*. Two transparency measures, the rate-hardness (1.29 *N/mm* and 2.16 *N/mm*) and the displayed stiffness (0.68 *N/mm* and 1.13 *N/mm*) are, however, became smaller. Note in this case that the dissipation capability parameter $\beta(n)$ is upper-bounded by B for all n because of a very stiff wall contact.

In comparison with the previous FBA[12] with *more conservative condition* whose control laws are as follows;

Table 1 The rate-hardness and displayed stiffness at each algorithm

		High velocity		Low velocity	
		Rate-hardness (*N/mm*)	Displayed stiffness (*N/mm*)	Rate-hardness (*N/mm*)	Displayed stiffness (*N/mm*)
Less conservative condition	Viscous damping	3.06	0.71	7.87	0.69
	Viscous damping + Coulomb friction	6.05	2.28	8.02	4.09
AOL		6.02	2.47	8.25	4.44
More conservative condition	Viscous damping	0.54	0.54	0.54	0.54
	Viscous damping + Coulomb friction	1.29	0.68	2.16	1.13

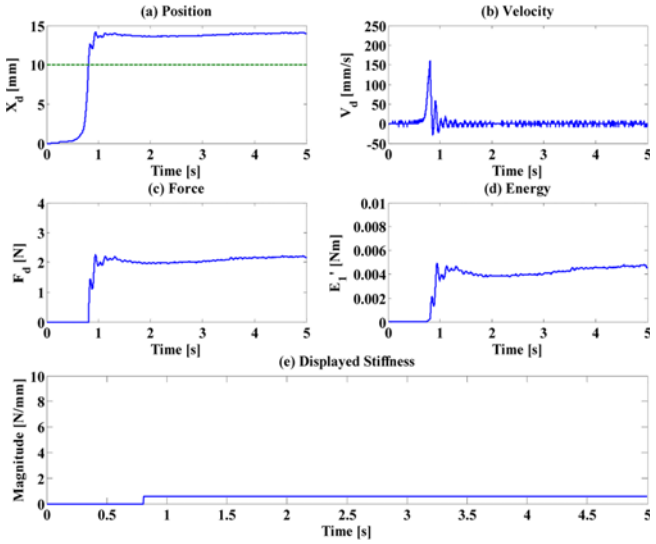

Fig. 16 Experimental results for large stiffness (k = 10 N/mm) with a *more conservative condition* using viscous damping at high velocity

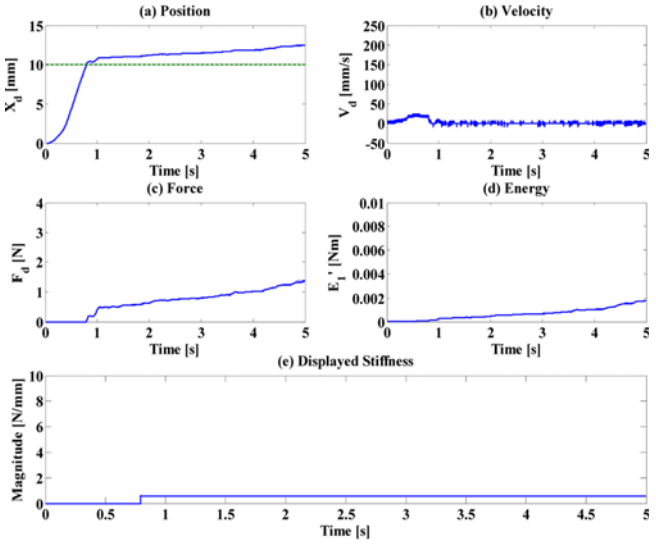

Fig. 17 Experimental results for large stiffness (k = 10 N/mm) with a *more conservative sufficient condition* using viscous damping at low velocity

$$\gamma(n) = 2\beta(n-1)\Delta x_d(n) + F_d(n-1), \tag{37}$$

$$\beta(n) = \frac{F_e^2(n)}{\gamma^2(n)}\beta(n-1) \quad for \quad F_e(n) \neq 0, \tag{38}$$

$$if\left(\beta(n) > B\right) \quad \beta(n) = B, \tag{39}$$

$$F_{\max}(n) = \sqrt{\frac{\beta(n)}{\beta(n-1)}\gamma^2(n)}, \qquad F_{\min}(n) = -\sqrt{\frac{\beta(n)}{\beta(n-1)}\gamma^2(n)}, \tag{40}$$

Figs. 16 and 17 show the experimental results with the rate-hardness of 0.54 *N/mm* and with the displayed stiffness of 0.54 *N/mm*. These values are smaller than those from the proposed *more conservative condition* because Coulomb friction term is not included.

Table 1 shows that for all cases of contacting very stiff virtual objects, the proposed enhanced FBA can increase the contact transparency significantly compared with the previous FBA that only considered viscous damping term. Table 1 also shows that the proposed *less conservative condition* can display contact transparency in terms of steady-state contact force and initial crispness similar to those of the AOL. Fig. 18 shows the time histories of both approaches based on experimental position data at Fig. 10(a). The AOL generates a slightly

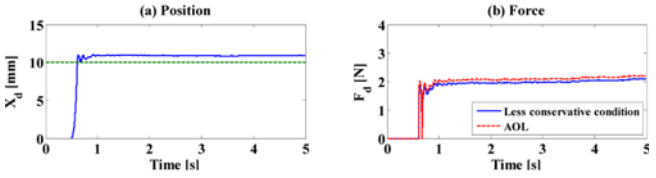

Fig. 18 Comparison between experimental results with a *less conservative condition* and simulated AOL based on experimental position data

greater force (5.9% increase). This clearly shows another validation that the proposed approximation to circumvent the causality problem in Eq. (12) has similar performance to the AOL approach that has not causality problem. That is, there is no stability problem but is only a slight reduction of transparency compared with the AOL.

Another simulation is performed for time-varying position input, *e.g.*, sinusoidal motion (with a frequency of 2 *Hz*) that can be used for palpation tasks. Fig. 19 shows stable force feedback for all three approaches. As already discussed, the AOL and the *less conservative condition* show larger displayed stiffness than the *more conservative condition*. Note that the displayed force slightly increases as time goes on for all methods. This is because of the force accumulation in Eqs.

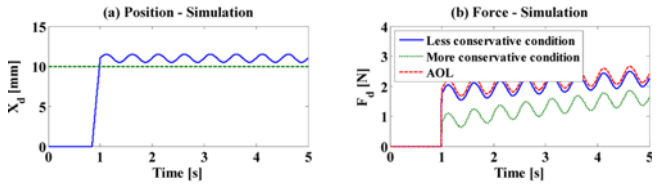

Fig. 19 Simulational results for varying position inputs

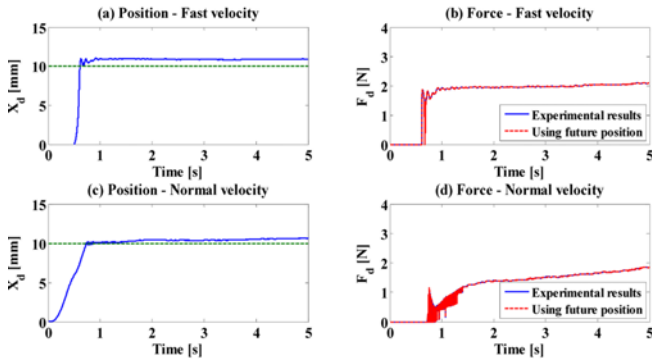

Fig. 20 Comparison between experimental results and original controller with a *less conservative condition* based on experimental position data

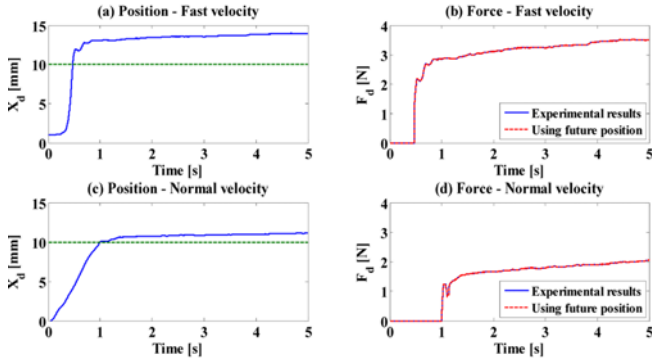

Fig. 21 Comparison between experimental results and original controller with a *more conservative condition* based on experimental position data

(14) and (30) from time-varying position input motion.

In order to avoid contact oscillations by the AOL and the proposed *less conservative condition*, a *more conservative condition* is used for systematically removing the past accumulated energy. The *more conservative condition*, however, reduces also the contact transparency magnitude significantly, which is a kind of trade-off between the initial contact realism and steady-state contact realism.

4.3 Post-verification

This section experimentally validates that the modification in the control laws in Eqs. (14) and (31) does not significantly affect the controlled force. Figs. 20 and 21 show the comparisons between experimental forces and original controlled forces by Eqs. (12) and (27) for each case based on experimental position information at Figs. 10(a), 11(a), 14(a) and 15(a). It shows almost the same values. More

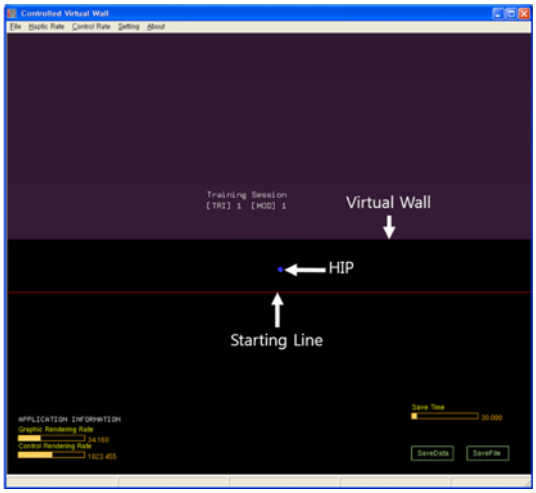

Fig. 22 The virtual environment for user study

comprehensive simulation results (not shown here for space limit) also show similar results for various virtual environments (small stiffness, large stiffness, time-varying, non-linear, and varying position inputs). Thus, no causality problem occurred with the proposed controller.

5. User Study

In order to confirm the influence of Coulomb friction in the proposed algorithm, a user-study is carried out. This experiment is performed only for the *more conservative condition* with and without Coulomb friction.

5.1 Participants

Ten participants (nine men; one woman) volunteered for this user study. Their average age was 25.7 years old (SD = 3.20 years). All subjects were right-handed and had normal vision, and reported that they had no health- or haptic-related problems.

5.2 Procedure

When individual participants arrived at the laboratory, they were informed about the goal of the experiment. Then, they participated in a training session to practice the perception task until they were familiar with the task and procedure. During the experiment, participants were touched the virtual wall using PHATNToM 1.5 with three fingers (thumb, index finger and middle finger) grip of their dominant hand. While they carried out the experiments, the white noise played through earphones to block any auditory information. In order to confirm the influence of Coulomb friction for two different velocity ranges of the operator's motion, this experiment contained the visual feedback to maintain the constant velocity of the haptic interaction point (HIP) as shown in Fig. 22 used by Zadeh.[19] The color of HIP informed the relationship between the participant's velocity and the reference velocity's range. If the velocity of the HIP between the starting line and the virtual wall is within the range of reference velocity, the color of HIP is blue. If this velocity is out of the reference ranges, the color is changed (Slow: yellow, Fast: red). Therefore, the operators can control their velocity based on HIP's color. The range of low velocity is 20~50 *mm/s*, and the

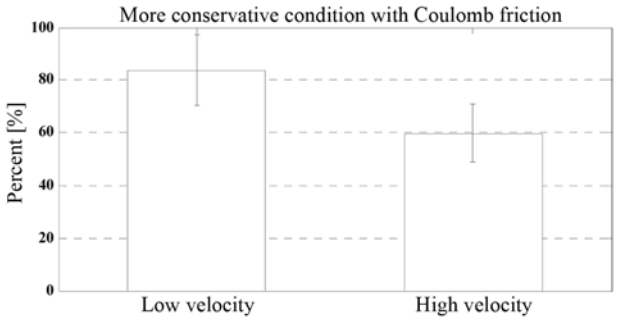

Fig. 23 Mean values with standard error bars

range of high velocity is 150~250 *mm*/*s*. After the training, participants were given a few minutes break and then the main session began.

The main session was similar to the training session, except for the number of trials to touch virtual wall. The two *more conservative conditions* (viscous damping term only and both viscous damping and Coulomb friction terms) are presented randomly for the large stiffness virtual wall at *y*-axis per each trial, it is 30 times trial respectively with visual feedback at each velocity range. Each participant, therefore, received a total of 120 stimuli. The participant chose which wall is stiffer than the other on each trial.

5.3 Results

Fig. 23 shows the experimental results from the user-study to choose the stiffer virtual wall. The most participants felt stiffer with the inclusion of Coulomb friction at the low velocity case (Mean = 83.67%, SD = 13.56%) and at the high velocity case (Mean = 59.67%, SD = 10.94%). In order to find out the reason, we analyzed more deeply and analytically the displayed stiffness for the more conservative passivity condition (See the Appendix below). The results show that the displayed stiffness is directly related to the penetration depth (see Eq. (42)) during the haptic interaction experiments. On the other hand, the experimental data in the user study results show that the penetration depth is usually small at the low velocity case (the average penetration depth of all users was 1.52 *mm*) as compared with the high velocity case (the average penetration depth of all users was 3.94 *mm*). In addition, the average displayed force $F_d(n)$ to the operator in the user study was 2.68 *N* at the high velocity case, and was 1.21 *N* at the slow velocity case. Therefore, the average displayed stiffness was 0.68 *N*/*mm* and 0.80 *N*/*mm* for the fast and slow velocity cases, respectively. Therefore, participants felt stiffer virtual wall at the low velocity case.

6. Conclusions and Future Works

This paper presented an enhanced force bounding approaches that included Coulomb friction as well as viscous damping of the haptic device to increase magnitude transparency more than that of the previous approach. Although the magnitude transparency is increased significantly by the proposed *less conservative condition* that is similar to AOL approach, these approaches usually induce severe contact oscillations due to the energy accumulation of dissipation capability during free motion. To reduce severe contact oscillations, the *more conservative condition* is also proposed for systematically removing the past accumulated energy. The approximation method to solve the causal problem does not affect stability, but only magnitude of transparency is degraded. The theory as well as experimental results showed that the proposed approaches can display interaction forces robustly stable and enhanced transparency while interacting with any virtual objects. The user-study also confirmed the influence of Coulomb friction.

Future investigations are planned to extend the approach to tool-based (six degrees-of-freedom) haptic interaction systems. For more transparency improvement, a simple way may be to add more physical damping that had been proposed by others.[20,21] More diverse real applications such as dental sculpting simulator will be tried in future.

ACKNOWLEDGEMENT

This work was supported by the GIST Research Institute (GRI).

REFERENCES

1. Lim, Y.-A., Lee, C.-G., Kim, J.-P., and Ryu, J., "Development of an AFM-Based Nanomanipulation System and Stable Haptic Interaction Using Modified Energy-Bounding Algorithm," Proc. of ICCAS-SICE, pp. 3798-3802, 2009.
2. Bolopion, A., Dahmen, C., Stolle, C., Haliyo, S., Régnier, S., and Fatikow, S., "Vision-Based Haptic Feedback for Remote Micromanipulation In-SEM Environment," International Journal of Optomechatronics, Vol. 6, No. 3, pp. 236-252, 2012.
3. Bolopion, A., Xie, H., Haliyo, D.S., and Régnier, S., "Haptic Teleoperation for 3-D Microassembly of Spherical Objects," IEEE/ASME Transactions on Mechatronics, Vol. 17, No. 1, pp. 116-127, 2012.
4. Ullah, F. and Park, K., "Development of A Surface-Based Virtual Dental Sculpting Simulator with Multimodal Feedback," Int. J. Precis. Eng. Manuf., Vol. 14, No. 4, pp. 577-587, 2013.
5. Colgate, J. E. and Schenkel, G., "Passivity of a Class of Sampled-Data Systems: Application to Haptic Interfaces," Proc. of American Control Conference, pp. 3236-3240, 1994.
6. Colgate, J. E., Stanley, M. C., and Brown, J. M., "Issues in the Haptic Display of Tool Use," Proc. of IEEE/RSJ International Conference on Intelligent Robots and Systems 95.'Human Robot Interaction and Cooperative Robots', pp. 140-145, 1995.
7. Hannaford, B. and Ryu, J.-H., "Time-Domain Passivity Control of Haptic Interfaces," IEEE Transactions on Robotics and Automation, Vol. 18, No. 1, pp. 1-10, 2002.
8. Kim, J.-P. and Ryu, J., "Robustly Stable Haptic Interaction Control Using an Energy-Bounding Algorithm," The International Journal of Robotics Research, Vol. 29, No. 6, pp. 666-679, 2010.
9. Lee, D. and Huang, K., "Passive-Set-Position-Modulation Framework for Interactive Robotic Systems," IEEE Transactions on Robotics,

Vol. 26, No. 2, pp. 354-369, 2010.

10. Ryu, J.-H. and Yoon, M.-Y., "Memory-Based Passivation Approach for Stable Haptic Interaction," IEEE/ASME Transactions on Mechatronics, Vol. 19, No. 4, pp. 1424-1435, 2014.
11. Diolaiti, N., Niemeyer, G., Barbagli, F., and Salisbury, J. K., "Stability of Haptic Rendering: Discretization, Quantization, Time Delay, and Coulomb Effects," IEEE Transactions on Robotics, Vol. 22, No. 2, pp. 256-268, 2006.
12. Abbott, J. J. and Okamura, A. M., "Effects of Position Quantization and Sampling Rate on Virtual-Wall Passivity," IEEE Transactions on Robotics, Vol. 21, No. 5, pp. 952-964, 2005.
13. Colonnese, N. and Okamura, A., "Stability and Quantization-Error Analysis of Haptic Rendering of Virtual Stiffness and Damping," The International Journal of Robotics Research, Vol. 35, No. 9, pp. 1103-1120, 2016.
14. Kim, J., Seo, C., Ryu, J., and Kim, J.-P., "Enhancing Rate-Hardness of Energy-Bounding Algorithm by Considering Coulomb Friction of Haptic Interface," Proc. of Haptics Symposium, pp. 157-160, 2010.
15. Lee, K. and Lee, D. Y., "Adjusting Output-Limiter for Stable Haptic Rendering In Virtual Environments," IEEE Transactions on Control Systems Technology, Vol. 17, No. 4, pp. 768-779, 2009.
16. Kim, J.-P., Baek, S.-Y., and Ryu, J., "A Force Bounding Approach for Multi-Degree-of-Freedom Haptic Interaction," IEEE Transactions on Mechatronics, Vol. 20, No. 3, pp. 1193-1203, 2015.
17. Geomagic, "Haptic Devices that Add the Sense of Touch to your Digital World," http://www.geomagic.com/en/products-landing-pages/haptic (Accessed 24 MAY 2017)
18. Lawrence, D. A., Pao, L. Y., Dougherty, A. M., Salada, M. A., and Pavlou, Y., "Rate-Hardness: A New Performance Metric for Haptic Interfaces," IEEE Transactions on Robotics and Automation, Vol. 16, No. 4, pp. 357-371, 2000.
19. Zadeh, M. H., Wang, D., and Kubica, E., "Perception-Based Lossy Haptic Compression Considerations for Velocity-Based Interactions," Multimedia Systems, Vol. 13, No. 4, pp. 275-282, 2008.
20. Mehling, J. S., Colgate, J. E., and Peshkin, M. A., "Increasing the Impedance Range of a Haptic Display by Adding Electrical Damping," Proc. of 1st Joint Eurohaptics Conference and Symposium on Haptic Interfaces for Virtual Environment and Teleoperator Systems, pp. 257-262, 2005.
21. Lim, Y.-A., Ahn, H.-S., and Ryu, J., "Analogue Input Shaper for Haptic Interfaces," IET Control Theory & Applications, Vol. 3, No. 12, pp. 1553-1564, 2009.

APPENDIX

The stiffness felt by the operator from the proposed more conservative passivity condition with Coulomb friction is, in fact, dependent on the penetration depth. This can be explained easily for very stiff virtual walls, in which case the bounding law in Eq. (30) is always applied. In this case, $\beta(n)$ in Eq. (29) is bounded by B and then the i^{th} force $F_d(i)$ can be simplified as

$$\begin{aligned} F_d(i) &= \sqrt{\{F_d(i-1) + 2B\Delta x_d(i)\}^2 + 4Bf_c|\Delta x_d(i)|} \\ &= \sqrt{\begin{bmatrix}2B\{\Delta x_d(1)+\cdots+\Delta x_d(i-1)\}+\omega(i-1)\\ +2B\Delta x_d(i)\end{bmatrix}^2 + 4Bf_c|\Delta x_d(i)|} \\ &= \sqrt{\left[2B\{\Delta x_d(1)+\cdots+\Delta x_d(i-1)+\Delta x_d(i)\}+\omega(i-1)\right]^2 + 4Bf_c|\Delta x_d(i)|} \\ &= \sqrt{\left[2Bx_p(i)+\omega(i-1)\right]^2 + 4Bf_c|\Delta x_d(i)|} \\ &= \sqrt{\begin{bmatrix}4B^2x_p^2(i)\\ +\omega^2(i-1)+4Bx_p(i)\omega(i-1)\\ +4Bf_c|\Delta x_d(i)|\end{bmatrix}} \\ &\quad 2Bx_p(i)+\omega(i) \end{aligned} \tag{41}$$

where the penetration depth $x_p(i) = \Delta x_d(1) + \ldots + \Delta x_d(i)$ and $\omega_1(i)$ is the force except $2Bx_p(i)$ in (41). Then, the displayed stiffness can be derived at the i^{th} step as

$$\begin{aligned} k_{Dis}(i) &= \frac{F_d(i)}{x_p(i)} \\ &= \sqrt{\frac{4B^2x_p^2(i)+\omega^2(i-1)+4Bx_p(i)\omega(i-1)+4Bf_c|\Delta x_d(i)|}{x_p^2(i)}} \\ &= \sqrt{4B^2+\frac{\omega^2(i-1)+4Bx_p(i)\omega(i-1)+4Bf_c|\Delta x_d(i)|}{x_p^2(i)}} \end{aligned} \tag{42}$$